Journal of Systems Engineering and Electronics
Vol. PP, No. 99, September 2023, pp.1 – 9

Detection method of forward-scatter signal based on Rényi entropy

ZHENG Yuqing, AI Xiaofeng*, YANG Yong, ZHAO Feng, and XIAO Shunping

State Key Laboratory of Complex Electromagnetic Environment Effects on Electronics and Information System, National University of Defense Technology, Changsha 410073, China

Abstract: The application scope of the forward scatter radar (FSR) based on the Global Navigation Satellite System (GNSS) can be expanded by improving the detection capability. Firstly, the forward-scatter signal model when the target crosses the baseline is constructed. Then, the detection method of the forward-scatter signal based on the Rényi entropy of time-frequency distribution is proposed and the detection performance with different time-frequency distributions is compared. Simulation results show that the method based on the smooth pseudo Wigner-Ville distribution (SPWVD) can achieve the best performance. Next, combined with the geometry of FSR, the influence on detection performance of the relative distance between the target and the baseline is analyzed. Finally, the proposed method is validated by the anechoic chamber measurements and the results show that the detection ability has a 10 dB improvement compared with the common constant false alarm rate (CFAR) detection.

Keywords: forward scatter radar (FSR), Global Navigation Satellite System (GNSS), time-frequency distribution, Rényi entropy, signal detection.

DOI: 10.23919/JSEE.2023.000122

1. Introduction

Passive radar based on the external radiation source has many advantages [1,2]. However, the target echo power may usually be too weak to be detected. Therefore, it is necessary to use long-time integration techniques or high-gain antennas [3−5], which makes the receiver complex and expensive. The passive radar based on the Global Navigation Satellite System (GNSS) has a wide coverage area and can work all weather and all day. However, the power density on the ground is too low (about −130 dBm), resulting in a very short detection range for GNSS-based passive radar [6−10].

The high-level radar cross section (RCS) can be obtained in the forward-scatter region. If forward-scatter detection is used, the detection range can be improved effectively. A forward scatter radar (FSR) network based on GNSS can be constructed through multiple distributed detection nodes on the ground, which can be used for aircraft detection [11]. In this way, it is urgent to find an effective detection method for the forward-scatter signal.

There are many research results on target detection for GNSS-based passive radar [12]. The received signal shows an obvious fluctuation [13−15], when the target crosses the baseline. Based on the echo extraction in the traditional tracking loop of the GNSS receiver, the received signal model was given in [16−18], and the shadow inverse synthetic aperture radar (SISAR) signal model and imaging method were established [19]. The forward-scatter signal of the civil airplane was captured in the experiment, and the experiment in [20] verified the feasibility of target detection in the FSR network.

The extracted forward-scatter signal is a two-sided chirped signal, which is similar to the linear frequency modulation (LFM) signal [21]. For the detection of LFM signal [22−24], time-frequency analysis, and Hough/Radon transform are usually used. It needs to perform the two-dimensional peak search, which is computationally intensive. It is especially important to find effective signal detection methods [25−28] combining the characteristics of forward-scatter signals.

In this paper, the geometry of GNSS-based FSR is constructed first, and the forward-scatter signal model is given. Then, the signal detection is realized by using the Rényi entropy of the time-frequency distribution, and the detection performance with different time-frequency distributions under constant false alarm rate (CFAR) conditions is compared. Finally, the detection algorithm is validated by the anechoic chamber measurements.

2. Forward-scatter signal model

The FSR baseline coordinate system is shown in Fig. 1, with the receiver at the origin and the transmitter at the

Manuscript received December 25, 2022.
*Corresponding author.
This work was supported by the National Natural Science Foundation of China (62071475; 61890541; 62171447).

y-axis. The target trajectory is parallel to the xOy plane, so the z-axis is perpendicular to the target trajectory and baseline, and the velocity is v. The distance from the intersection point of the target trajectory projection on the xOy plane and the baseline to the origin is d_{R}. The three-dimensional position coordinates of the rectangular target (length l × width h) are $(x(t), y(t), z_{\mathrm{p}})$, where z_{p} is the target height relative to the xOy plane, and is also the shortest distance from the target trajectory to the baseline. The intersection angle between the target trajectory projection and the baseline is θ_{t}. The angles α_{h}, α_{v} and β_{h}, β_{v} represent the azimuth and elevation of the target relative to the receiver and transmitter, respectively. R_{T} represents the distance between the target and the satellite, R_{R} represents the distance between the target and the receiver, and L represents the distance between the satellite and the receiver.

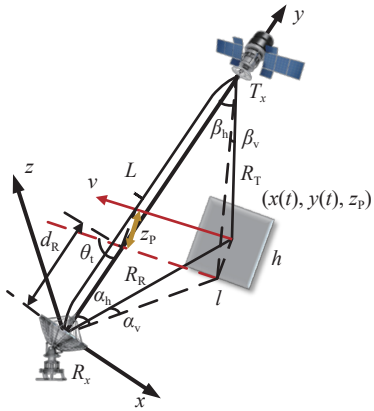

Fig. 1 Geometry of GNSS-based FSR

Under the forward-scatter detection structure, the received signal can be regarded as the coherent superposition of direct wave and target scattered wave. After down-conversion and code/carrier tracking, the expression of the extracted forward-scatter signal is given in [16−18] as

$$E(t)=U_{\mathrm{tg}}(t)\cos\left[\varphi_{\sigma}-\frac{2\pi f_0}{\mathrm{c}}\left(R_{\mathrm{T}}(t)+R_{\mathrm{R}}(t)-L(t)\right)\right] \tag{1}$$

where $U_{\mathrm{tg}}(t)$ is the target scattered signal amplitude, depending on the target shape and target position, φ_{σ} is the target scattered phase, f_0 is the carrier frequency, and c is the velocity of light.

The Doppler frequency is the difference between the Doppler frequency of the target scattered signal and that of the direct signal. $U_{\mathrm{tg}}(t)$ can be calculated as

$$U_{\mathrm{tg}}(t)=\sqrt{2P_{\mathrm{r}}(t)}=\sqrt{\frac{2P_{\mathrm{E}}G_{\mathrm{R}}\sigma_{\mathrm{fs}}(t)\lambda^2}{(4\pi)^3R_{\mathrm{T}}^2(t)R_{\mathrm{R}}^2(t)}} \tag{2}$$

where $P_{\mathrm{r}}(t)$ represents the target scattered signal power, P_{E} is the equivalent omnidirectional radiation power (including antenna gain) of the GNSS satellite, G_{R} is the receiving antenna gain, σ_{fs} is the target forward-scatter RCS, and λ is the signal wavelength.

The forward-scatter RCS of the rectangular target [29] can be calculated as

$$\sigma_{\mathrm{fs}}(t)=4\pi\frac{(lh)^2\sin(\theta_{\mathrm{t}}-\beta_{\mathrm{h}})\cos^2\beta_{\mathrm{v}}}{\lambda^2}\cdot\left(\mathrm{sinc}\left(\frac{\pi\, l\sin(\theta_{\mathrm{t}}-\beta_{\mathrm{h}})}{\lambda}\sin(\alpha_{\mathrm{h}}+\beta_{\mathrm{h}})\right)\right)^2\cdot\left(\mathrm{sinc}\left(\frac{\pi\, h\cos\beta_{\mathrm{v}}}{\lambda}\sin(\alpha_{\mathrm{v}}+\beta_{\mathrm{v}})\right)\right)^2. \tag{3}$$

In the FSR baseline coordinate system, (1) is approximately expressed as

$$E_{\mathrm{r}}(t)\approx U_{\mathrm{tg}}(t)\cos\left[\pi\, K_{\mathrm{r}}'t^2+\pi\, z_{\mathrm{P}}^2/(d_{\mathrm{R}}\lambda)-\varphi_{\sigma}\right] \tag{4}$$

where K_{r}' is the Doppler rate in Hz/s, expressed as

$$K_{\mathrm{r}}'=\frac{v^2\sin^2\theta_{\mathrm{t}}}{d_{\mathrm{R}}\lambda}. \tag{5}$$

In summary, the phase contains information such as the distance d_{R} from the target crossing position to the receiver and the minimum distance z_{p} from the target to the baseline. The frequency modulation includes information such as target velocity v and motion direction θ_{t}. The change of these parameters will influence the detection performance, especially the values of d_{R} and z_{p} are related to the power of the target scattered signal.

Although the target can obtain a high level of RCS in the forward-scatter area, coherent/incoherent integration is still required to improve the signal to noise ratio (SNR). Due to the limitations of the forward-scatter condition, the target is in the detectable range for a short time, and it is challenging to achieve target detection and motion parameter estimation in this period. The signal parameters, including Doppler slope and scattering phase, are determined by the target motion state, so the signal waveform cannot be known in advance. It is difficult to obtain the prior knowledge required for traditional detection quantity design. Thus the usual incoherent energy integration method is used. However, when the SNR is low, the noise energy will also be accumulated, which leads to that the method cannot work very well. In the next section, the signal detection method based on the Rényi entropy of time-frequency distribution [30] is introduced, which does not require energy accumulation and avoids this problem effectively.

3. Signal detection based on Rényi entropy of time-frequency distribution

Entropy is a measurement of the “uncertainty” of a system. The concept of Rényi entropy of time-frequency distribution [30] is defined as

$$H_\alpha(C_s(n,k)) = \frac{1}{1-\alpha}\log_2 \sum_{n=-N}^{N}\sum_{k=-K}^{K}\left(\frac{C_s(n,k)}{\sum_{n'k'} C_s(n',k')}\right)^\alpha \quad (6)$$

where N is the number of sampling time points, K is the number of sampling frequency points, $\alpha > 0$ is the order of Rényi entropy, and $C_s(n,k)$ is the time-frequency distribution corresponding to signal $s(n)$.

The Rényi entropy reflects the amount of information contained in the time-frequency distribution. Because the noise is a random signal, its time-frequency distribution contains a large amount of information. We can use the Rényi entropy of the time-frequency distribution as the detection statistic quantity. For different kernel functions, the entropy values are different. To make the entropy value smaller and have a good distinction with the noise, it is necessary to minimize the complexity of the time-frequency distribution.

According to the detection theory, the decision criterion is

$$H_\alpha(C_s(n,k)) \underset{H_1}{\overset{H_0}{\gtrless}} \gamma \quad (7)$$

where γ is the threshold of judgment.

The judgment criterion is expressed as

$$X = \sum_{k=-K}^{K}\sum_{n=-N}^{N}\left(\frac{C(n,k)}{\sum_{n'}\sum_{k'} C(n',k')}\right)^\alpha \underset{H_1}{\overset{H_0}{\gtrless}} \eta \quad (8)$$

where $\eta = 2^{(1-\alpha)\gamma}$.

According to the central limit theorem, for a sufficient number of sampling time points N and sampling frequency points K, X approximately obeys the normal distribution with mean value m and standard deviation σ.

The false alarm probability of detection can be expressed as

$$P_f = Q\left(\frac{\eta - m}{\sigma}\right) \quad (9)$$

where $Q(x) = \int_x^{+\infty} \frac{1}{\sqrt{2\pi}}\exp\left(-\frac{1}{2}t^2\right)dt$ is the right-tailed probability function of the random variable.

Therefore, the judgment threshold is

$$\eta = \sigma Q^{-1}(P_f) + m. \quad (10)$$

After 10^4 Monte Carlo simulations, the detection statistics of noise-containing forward-scatter signal are calculated and its distribution is showed in Fig. 2. The flow chart of simulation validation is summarized in Fig. 3. First, the SNR parameter is set, Monte Carlo simulations for the case only with noise are conducted, and the normal distribution curve is used to fit the detection statistic X. The mean value m and the standard deviation σ can be estimated, so the decision threshold η can be obtained. Then, based on (4), the signal containing forward-scatter signal and noise is simulated by Monte Carlo for equal times to determine the detection probability. Changing the parameters, the above process is repeated to obtain the detection probability with different SNRs.

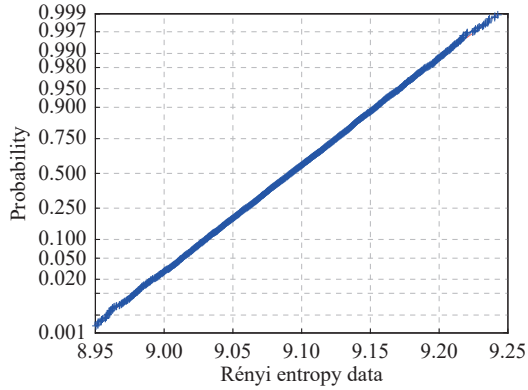

Fig. 2 Test of normal distribution of statistics

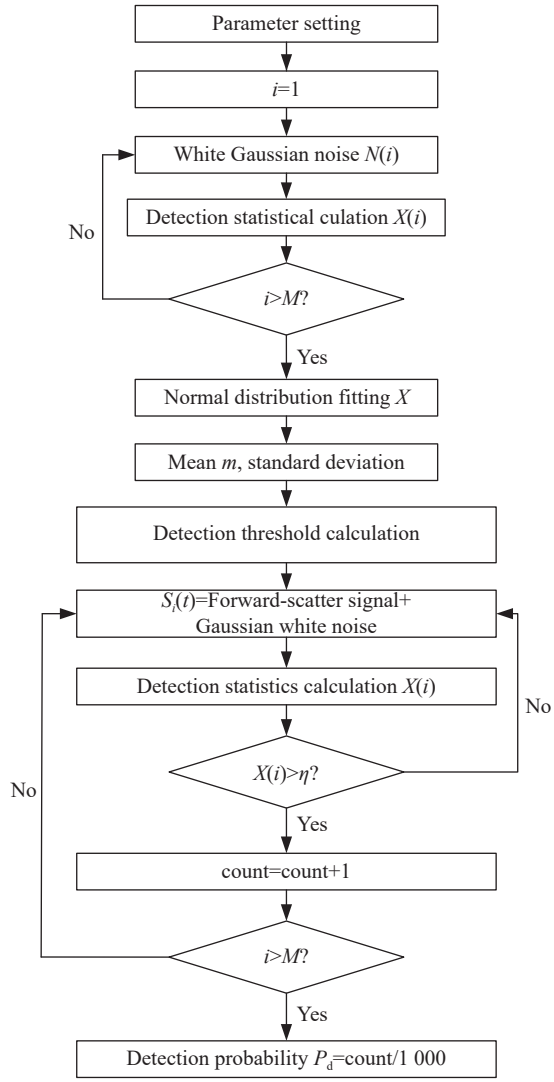

Fig. 3 Simulation validation based on the Rényi entropy of time-frequency distribution

4. Simulation and analysis

In the real scene, the received signal includes forward-scatter signal, multipath signal, noise, and interference. The multipath signal can be removed by adding a window in the linear canonical transform domain [31]. The forward-scatter signal simulation using (4) in this section only considers noise. The parameters are shown in Table 1. The time domain waveform of the forward-scatter signal is shown in Fig. 4(a), and the target RCS calculated with (3) is shown in Fig. 4(b), which shows that the signal amplitude is modulated by RCS, and the signal is symmetrical about the crossing time. The SPWVD of the forward-scatter signal is shown in Fig. 4(c). The forward-scatter signal is approximately the LFM signal.

Table 1 Simulation parameters of forward-scatter signal

Parameter	Symbol	Value
Omnidirectional radiation power/dBw	P_{E}	30
Receiving antenna gain/dB	G_{R}	10
Carrier frequency/MHz	f_0	1 268.52
Baseline length/km	R_{D}	21 528
Target scattered phase/rad	φ_σ	$3\pi/2$
Rectangle target length/m	l	20
Rectangle target width/m	h	13
The distance between the target crossing point and the receiver/m	d_{R}	8 000
The angle between the target motion direction and baseline/rad	θ_{t}	$\pi/2$
Target velocity/(m·s^{-1})	v	250
The minimum distance between the target trajectory and the baseline/m	z_{p}	0
Signal sampling frequency/Hz	f_{s}	100
False alarm probability	P_{f}	10^{-6}

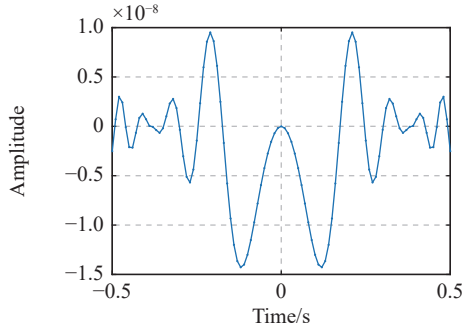

(a) Forward-scatter signal

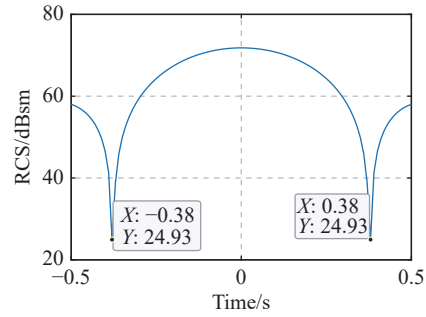

(b) Target forward-scatter RCS

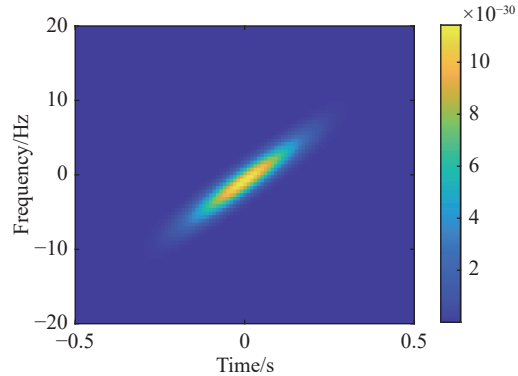

(c) SPWVD of forward-scatter signal

Fig. 4 Simulation results of forward-scatter signal

4.1 Detection performance with different time-frequency distributions

The selected time-frequency transformation methods include pseudo Wigner-Ville distribution (PWVD), SPWVD, Born Jordan distribution (BJD), Margenau Hill distribution (MHD), Choi Williams distribution (CWD) and Butterworth distribution. The SPWVD expression is

$$\mathrm{SPW}_x(t,f)=\int_{-\infty}^{+\infty}h(\tau)\int_{-\infty}^{+\infty}g(s-t)x\left(s+\frac{\tau}{2}\right)x^*\left(s-\frac{\tau}{2}\right)\mathrm{e}^{-\mathrm{j}2\pi f\tau}\mathrm{d}s\mathrm{d}\tau \quad (11)$$

where $x(t)$ represents the forward-scatter signal, $g(s-t)$ is a smooth window function in the frequency domain; $h(t)$ is a smooth window function in the time domain; $g(0)=h(0)=1$. The rest of the time-frequency distribution is defined in [32].

The times of Monte Carlo simulations is set as 1 000, as shown in Fig. 5(a). The Rényi entropy is also calculated for noise signals with different SNRs, as shown in Fig. 5(b), which proves that the forward-scatter signal detection can be realized by using the difference of Rényi entropy.

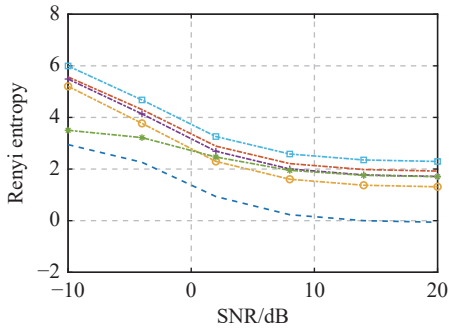

(a) Rényi entropy of forward-scatter signal and noise

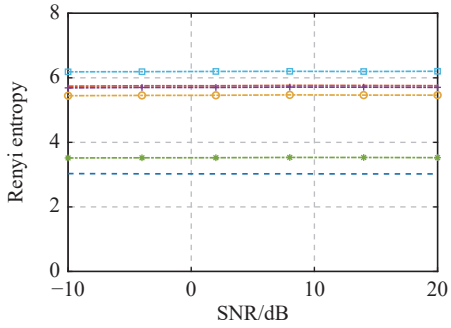

(b) Rényi entropy of noise

: PWVD; : BJD; : MHD; : CWD; : Butterworth; : SPWVD.

Fig. 5 Rényi entropy under different time-frequency distributions

Set the order of Rényi entropy as 3, the times of Monte Carlo simulations as 10^4, and the signal duration as 1 s. The detection probability curves are shown in Fig. 6. The detection probability with the SPWVD is the highest and the MHD is the worst. When SNR = −3 dB, the detection probability with almost all the time-frequency distributions exceeds 80%, which has great advantages over the 12 dB requirements of conventional CFAR detection. Therefore, the detection range can be further expanded by selecting the proposed detection method for the GNSS-based FSR.

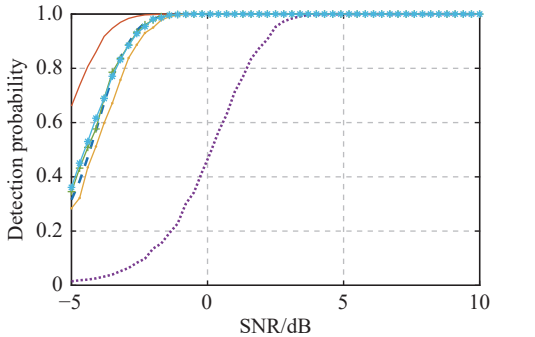

: PWVD; : BJD; : CWD; : SPWVD; : PMH; : Butterworth.

Fig. 6 Detection probability under different time-frequency distributions (false alarm rate is 10^{-6})

4.2 Detection performance analysis with different signal parameters

According to the forward-scatter signal model, the signal parameters, affecting the detection performance, include the distance d_R from the projection point on the baseline to the receiver, the shortest distance z_p from the baseline when the target crosses, the angle θ_t between the target trajectory and the baseline, and the target velocity v. In addition, the motion process when the target is gradually approaching the baseline also affects the detection performance. In the real application, a segment of the received signal is chosen to detect whether there is a target echo. Assuming that the vertical distance from the midpoint of the target trajectory corresponding to the signal segment to the baseline is d, and the impacts of z_p and d values on the detection performance are analyzed as follows.

Fig. 7 shows the detection probability with different z_p. In Fig. 7(b), when z_p reaches 35 m, the detection probability decreases quickly, which is caused by the modulation of the target RCS on the signal amplitude. The target RCS can be regarded as a sinc function, and then it reaches the first zero point. With the increase of z_p, the corresponding bistatic angle gradually decreases, and the RCS value changes as the side lobe. The RCS drops sharply, so the detection probability decreases. As the length of the signal segment increases, the signal energy becomes larger, and the peak value of detection probability becomes larger after $z_p > 50$ m. Under the current system parameters, the detection range near the baseline is 35 m, and a larger detection range can be obtained by extending the signal integration time and using a high-gain antenna.

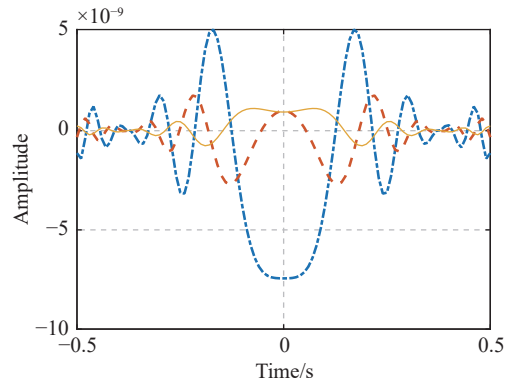

: z_p=30 m; : z_p=60 m; : z_p=100 m.

(a) Forward-scatter signal with different z_p

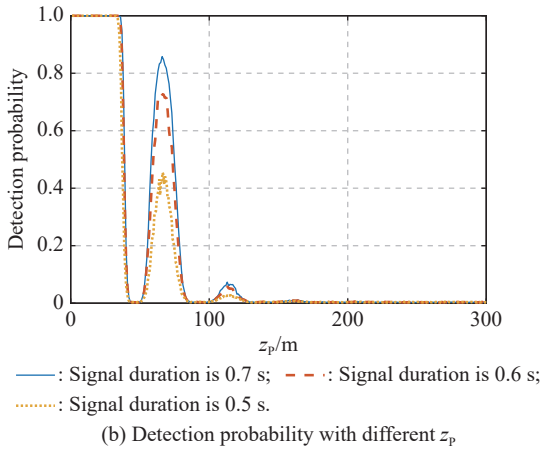

(b) Detection probability with different z_p

Fig. 7 Detection probability analysis

Fig. 8 shows the detection probability with different d. Starting with the case that the target trajectory is symmetrical about the baseline (d = 0 m). The signal segment is intercepted using a sliding window with the length set to 0.5 s, 0.6 s, and 0.7 s, respectively. And the sliding length is 0.02 s. With the increase of d, the corresponding position in the center of the signal segment is gradually away from the baseline. With the same receiver noise, the SNR is gradually reduced. Therefore, Fig. 8 shows a downward trend. When $d \approx 150$ m, the corresponding moment of the signal segment center is about 0.6 s. At this time, the detection curve is stable near a certain value, and the RCS value corresponding to the signal segment is gradually away from the main lobe. The greater the length of the signal segment, the greater the detection probability stability value. When d reaches about 200 m, the central moment of the signal segment is 0.8 s, which corresponds to the RCS slide lobe area, so the detection probability drops sharply.

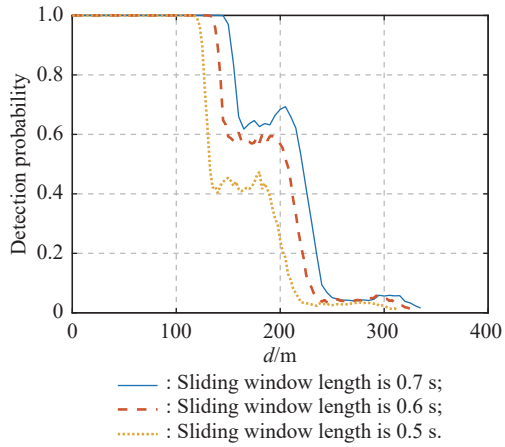

Fig. 8 Detection probability with different *d*

5. Experimental validation

5.1 Anechoic chamber experiment design

To obtain the forward-scatter signal, we make the target pass through the line between the transmitting and receiving antennas with a uniform velocity. The target height should be adjustable, so we can obtain the target echoes with different heights. The designed experiment scenario is shown in Fig. 9, where H_T and H_R are the heights from the transmitting antenna and receiving antenna to the ground, respectively, and H is the height from the target center to the ground. The motion direction of the target is consistent with the slide rail direction, and θ_t is the angle between the target motion track and the baseline. d_T and d_R are the distances from the intersection point of the target track and the baseline to the transmitter and receiver respectively. The target size is $l \times h$ m^2, R_D is the baseline length.

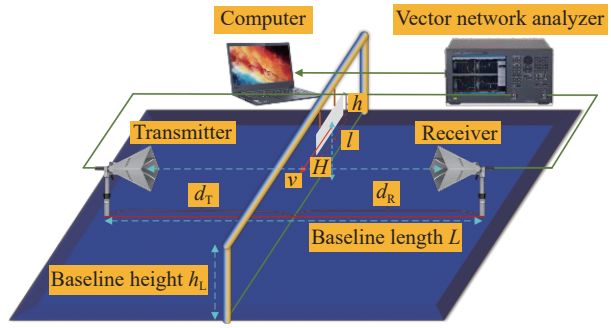

Fig. 9 Design drawing of the experiment scene

The measure system consists of absorbing materials, an aluminum plate target, an electric booster, a slide rail, a radar transmitting/receiving antenna (with 20° beam width) and a vector network analyzer. The experimental scene is shown in Fig.10. After the experiment scene is built, we start the vector network analyzer to transmit and receive the signal. The system parameter settings in the experiment are shown in Table 2.

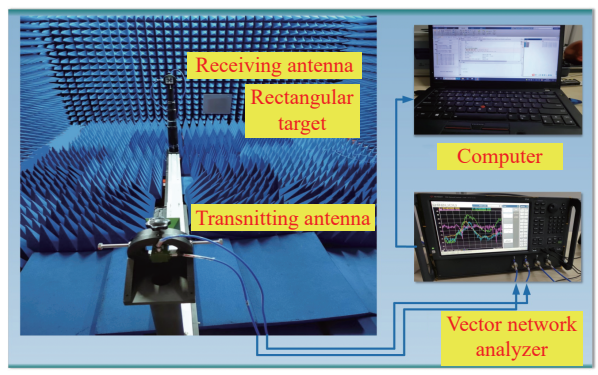

Fig. 10 Experimental scene in the anechoic chamber

Table 2 Experimental parameters

Parameter	Value
Target size($l\times h$)/cm^2	13×13
Target height H/m	1.21−1.46
Height of transmitting antenna H_T/m	1.21
Height of receiving antenna H_R/m	1.21
Polarization	HH
Frequency/GHz	10
Testing time/s	23.7
θ_t/(°)	90
d_T/m	1.16
v/(m·s^{-1})	0.14
R_D/m	2.36

5.2 Experimental results analysis

For the aluminum plate target, the electric booster is used to make the target pass through the line between the transmitting antenna and the receiving antenna, the vector network transmits the stepping frequency signal (the frequency is 8−12 GHz). The direct signal amplitude is calculated with the average value of the received signal amplitude without the target. The received signal after the removal of the direct wave at the frequency point of 10 GHz is given in Fig. 11(a), which can be approximately considered that z_p = 0 m and the target accurately crosses the baseline. To use the most concentrated part of the signal energy for detection, the signal segment of 9−15 s is intercepted, and its time-frequency distribution is shown in Fig. 11(b).

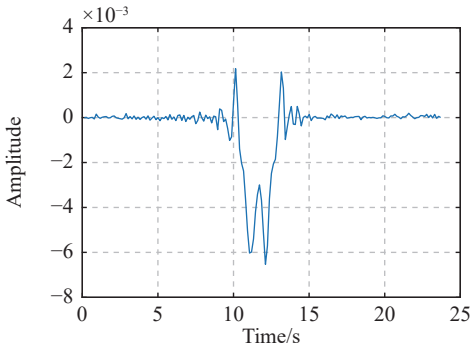

(a) Measurement results

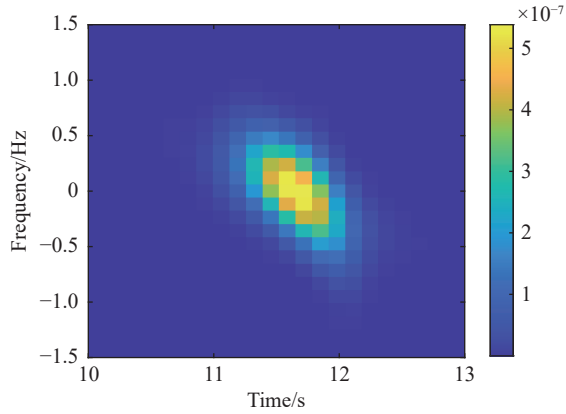

(b) Time-frequency diagram of measurement data

Fig. 11 Analysis of measurement data

Six sets of data are measured with different target heights. The measured data are considered as the noise-free signal, and noise is added to obtain the detection probabilities at different SNRs with 5 000 Monte Carlo times, as shown in Fig. 12. When the SNR reaches −3 dB, the detection probability reaches 83%, which has worse performance than that in Fig. 6, because the original measurement data contains background noise.

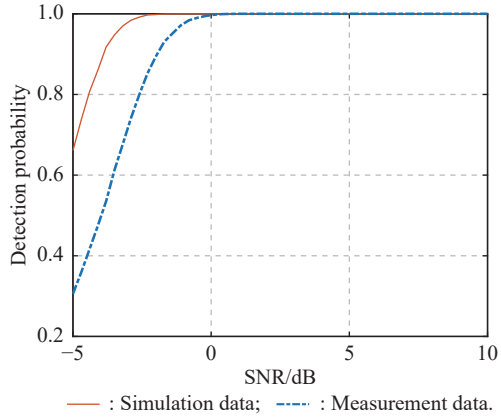

Fig. 12 Detection probability using SPWVD (false alarm rate is 10^{-6})

We add noise to the original measurement data so that the SNR is 0 dB, when z_p = 0 m or d = 0 m. In other cases, the received signal is added with equal white Gaussian noise. The number of Monte Carlo times is 10^4. Results are shown in Fig. 13. With the increase of z_p and d from zero, the detection probability shows a decreasing trend, which is consistent with the simulation results when z_p < 35 m, proving the correctness of the theoretical analysis.

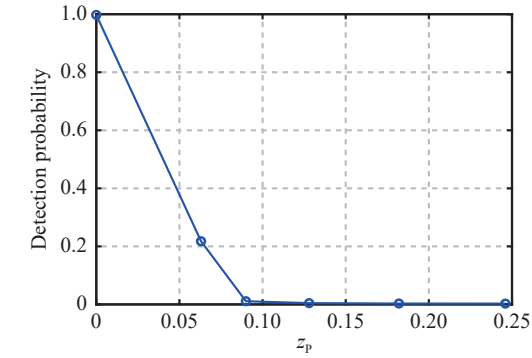

(a) Detection probability under different z_P

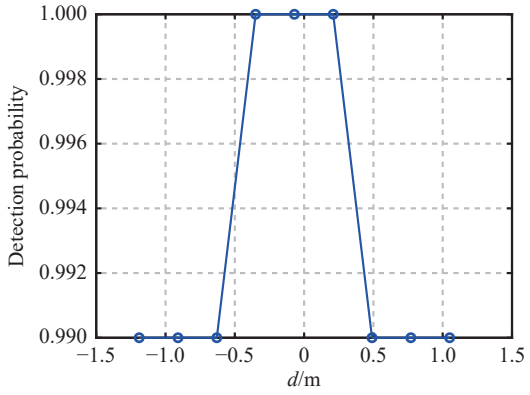

(b) Detection probability under different d

Fig. 13 Detection performance analysis under different parameters (false alarm rate 10^{-6}, SPWVD)

6. Conclusions

In this paper, the GNSS-based FSR signal model that the target crosses the baseline is induced. Aiming at the problem of forward-scatter signal detection, a detection method based on the rényi entropy of time-frequency distribution is proposed. The results show that the detection performance of the method based on SPWVD distribution is the best when the false alarm rate is 10^{-6}. When the SNR is 0 dB, the detection probability reaches 99%. Compared with the conventional CFAR detection method, it can effectively improve the detection range. In addition, the method can adapt to the scene where the target deviates from the baseline, which lays a foundation for subsequent signal parameter estimation and target parameter estimation. In the next step, research on the estimation methods of the signal parameter based on detection results will be carried out.

References

[1] SONG J, XIONG W, CHEN X L, et al. Experimental study of maritime moving target detection using hitchhiking bistatic radar. Remote Sensing, 2022, 14(15): 3611.

[2] ZHANG Z X, ZHENG Y, ZHENG L H, et al. Range resolution and sampling frequency trade-off for GPS passive radar. Journal of Systems Engineering and Electronics, 2022, 33(1): 28–37.

[3] LI X L, YANG Y C, SUN Z, et al. Multi-frame integration method for radar detection of weak moving target. IEEE Trans. on Vehicular Technology, 2021, 70(4): 3609–3624.

[4] ZHU S Q, LIAO G S, YANG D, et al. A new method for radar high-speed maneuvering weak target detection and imaging. IEEE Geoscience and Remote Sensing Letters, 2013, 11(7): 1175–1179.

[5] CHEN X L, HUANG Y, GUO J, et al. Review of long-time integration techniques for weak targets using MIMO radar. Journal of Signal Processing, 2020, 36(12): 1947–1964.

[6] MA H, ANTONIOU M, STOVE A G, et al. Maritime moving target localization using passive GNSS-based multistatic radar. IEEE Trans. on Geoscience and Remote Sensing, 2018, 56(8): 4808–4819.

[7] ANTONIOU M, STOVE A G, TZAGKAS D, et al. Marine target localization with passive GNSS-based multistatic radar: experimental results. Proc. of the International Conference on Radar, 2018. DOI: 10.1109/RADAR.2018.8557331.

[8] MA H, ANTONIOU M, PASTINA D, et al. Maritime moving target indication using passive GNSS-based bistatic radar. IEEE Trans. on Aerospace and Electronic Systems, 2018, 54(1): 115–130.

[9] SANTI F, PIERALICE F, PASTINA D. Joint detection and localization of vessels at sea with a GNSS-based multistatic radar. IEEE Trans. on Geoscience and Remote Sensing, 2019, 57(8): 5894–5913.

[10] SANTI F, PASTINA D, BUCCIARELLI M. Experimental demonstration of ship target detection in GNSS-based passive radar combining target motion compensation and track-before-detect strategies. Sensors, 2020, 20(3): 599.

[11] AI X F, ZHENG Y Q, XU Z M, et al. Parameter estimation for uniformly accelerating moving target in the forward scatter radar network. Remote Sensing, 2022, 14(4): 1006.

[12] SUBERVIOLA I, MAYORDOMO I, MENDIZABAL J. Experimental results of air target detection with a GPS forward-scattering radar. IEEE Geoscience and Remote Sensing Letters, 2012, 9(1): 47–51.

[13] KABAKCHIEV H, GARVANOV I, BEHAR V, et al. Experimental verification of target shadow parameter estimation in GPS FSR. Proc. of the 17th International Radar Symposium, 2016. DOI: 10.1109/IRS.2016.7497337.

[14] HU C, LIU C J, ZENG T. Bistatic forward scattering radar detection and imaging. Journal of Radars, 2016, 5(3): 229–243.

[15] KABAKCHIEV H, GARVANOV I, BEHAR V, et al. Multichannel target shadow detection in GPS FSR. Cybernetics and Information Technologies, 2019, 19(1): 116–132.

[16] LIU C J, HU C, ZENG T, et al. Signal modeling and experimental verification in GNSS forward scatter radar. Proc. of the 17th International Radar Symposium, 2016. DOI: 10.1109/IRS.2016.7497340.

[17] HU C, LIU C J, WANG R, et al. Detection and SISAR imaging of aircrafts using GNSS forward scatter radar: signal modeling and experimental validation. IEEE Trans. on Aerospace and Electronic Systems, 2017, 53(4): 2077–2093.

[18] LIU C J, HU C, WANG R, et al. GNSS forward scatter radar detection: signal processing and experiment. Proc. of the 18th International Radar Symposium, 2017: 1−9.

[19] HU C, WANG L, LIU C J. SISAR imaging method based on GNSS signal: theory and experimental results. Proc. of the CIE International Conference on Radar, 2016. DOI: 10.1109/RADAR.2016.8059223.
[20] WACHTL S, KOCH V, SCHMIDT L P. Multipath sensor based on GNSS for passive airborne surveillance. Proc. of the European Radar Conference, 2013: 255−258.
[21] CHEN X L, JIANG Q W, SU N Y, et al. LFM signal detection and estimation based on deep convolutional neural network. Proc. of the Asia-Pacific Signal and Information Processing Association Annual Summit and Conference, 2019: 753−758.
[22] SUN Q, ZHANG Y, WEI Y, et al. A novel multicomponent LFM signal detection based on fast block FRFT. Proc. of the IET International Radar Conference, 2020: 1090−1094.
[23] ZHANG Z G. Linear canonical wigner distribution based noisy LFM signals detection through the output SNR improvement analysis. IEEE Trans. on Signal Processing, 2019, 67(21): 5527–5542.
[24] WANG X C, DAN R. LFM signal perception based on wavelet transform and time-frequency technology. Proc. of the IEEE 16th International Conference on Signal Processing, 2022: 11−15.
[25] LI W H, WANG K R, YOU L, et al. A new deep learning framework for HF signal detection in wideband spectrogram. IEEE Signal Processing Letters, 2022, 29: 342–1346.
[26] XU C, HE Z, LIU H C, et al. Bayesian track-before-detect algorithm for nonstationary sea clutter. Journal of Systems Engineering and Electronics, 2021, 32(6): 1338–1344.
[27] JANG J A, LEE S I, SIM Y J, et al. Vital signal detection for continuous-wave radar sensor using compensation technique. Proc. of the IEEE International Symposium on Radio-Frequency Integration Technology, 2022: 115−117.
[28] DONG Y N, WU C Z, ZHU H Z, et al. A weak signal detection method based on spatial spectrum-LSTM neural network. Proc. of the 5th International Conference on Information Communication and Signal Processing, 2022. DOI: 10.1109/ICICSP55539.2022.10050602.
[29] GASHINOVA M, DANIEL L, SIZOV V, et al. Phenomenology of Doppler forward scatter radar for surface targets observation. IET Radar, Sonar & Navigation, 2013, 7(4): 422–432.
[30] LIANG Z Y. Detection based on the Rényi entropy of time-frequency distribution. Xi'an: Xidian University, 2007. (in Chinese)
[31] LIU M Q, ZHANG Z J, CHEN Y F, et al. Forward scatter radar meets satellite: passive sensing of aerial target using satellite communication waveforms. Remote Sensing, 2022, 14(6): 1375.
[32] COHEN L. Time frequency analysis. Upper Saddle River: Prentice Hall, 1995.

Biographies

ZHENG Yuqing was born in 1998. She received her M.S. degree from National University of Defense Technology in 2022. Her research interests include radar target location.
E-mail: zhengyuqing@nudt.edu.cn

AI Xiaofeng was born in 1983. He received his B.S. and Ph.D. degrees from National University of Defense Technology (NUDT) in 2005 and 2013, respectively. He is currently a lecturer with NUDT. His research interests include radar imaging and feature extraction
E-mail: anxifu2001@163.com

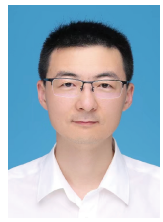

YANG Yong was born in 1985. He received his B.S. and Ph.D. degrees from National University of Defense Technology (NUDT). He is currently an associate professor with NUDT. His research interests include polarization radar target detection and anti-jamming.
E-mail: youngt_fvc@163.com

ZHAO Feng was born in 1978. He received his B.S. and Ph.D. degrees from National University of Defense Technology (NUDT) in 2001 and 2007, respectively. He is currently a professor with NUDT. His research interests include radar system design.
E-mail: zhfbee@tom.com

XIAO Shunping was born in 1964. He received his B.S. and Ph.D. degrees from National University of Defense Technology (NUDT) in 1986 and 1995, respectively. He is currently a professor with NUDT. His research interests include radar target recognition and radar signal processing.
E-mail: xiaoshunping_nudt@163.com